Title
Von Hippel Lindau negative tumor cell-derived exosomes in metastatic kidney cancer

Author
Flora, Kailey

Publication Date
2022

Peer reviewed|Thesis/dissertation

UNIVERSITY OF CALIFORNIA

Los Angeles

Von Hippel Lindau negative tumor cell-derived exosomes in metastatic kidney cancer

A thesis submitted in partial satisfaction

of the requirements for the degree Master of Science

in Bioengineering

by

Kailey Kimiko Flora

2022

ABSTRACT OF THE THESIS

Von Hippel Lindau negative tumor cell-derived exosomes

in metastatic kidney cancer

by

Kailey Kimiko Flora

Master of Science in Bioengineering

University of California, Los Angeles, 2022

Professor Lily Wu, Chair

Metastatic Renal Cell Carcinoma(RCC) has limited safe and effective treatments available. This is due to a lack of understanding relating to the mechanism of distant cancer metastasis. Metastatic crosstalk occurs between pseudo-hypoxic von Hippel-Lindau(VHL) knockout tumor cells and VHL wildtype tumor cells. VHL knockout cells have increased production of exosomes due to their pseudo-hypoxic state to help cells adapt to hypoxic conditions. VHL knockout-derived exosomes increase the metastatic properties of VHL wildtype recipient cells. Metastatic properties such as migration and metastasis occur in response between isolated exosomes from the CRISPR

modified VHL(-) Renca murine line and VHL(+) cells, generating a model of RCC metastasis and the potential to develop targeted diagnostics and therapeutics for metastatic disease.

The thesis of Kailey Kimiko Flora is approved.

Hsian-Rong Tseng

Daniel Kamei

Lily Wu, Committee Chair

University of California, Los Angeles

2022

TABLE OF CONTENTS

ABBREVIATIONS

RCC - renal cell carcinoma

ccRCC - clear cell renal cell carcinoma

VHL - von Hippel Lindau gene

VHL(+) cells - tumor cells with wildtype VHL gene

VHL(+)-LoxP cells - tumor cells with wildtype VHL and LoxP RFP modification

VHL(-) - tumor cells with knockout of VHL gene

VHL(-)-Cre - tumor cells with knockout of VHL gene and Cre recombinase vesicle modification

Exo - exosomes derived by preceding cell type

dCAM - duck chorioallantoic membrane model

LIST OF FIGURES AND SCHEMATICS

ACKNOWLEDGMENTS

I would like to express my deepest gratitude to Dr. Lily Wu, my supervisor, who has guided me during this project. Special thanks to Dr. Junhui Hu, Dr. Zhicheng Zhang, and Moe Ishihara for training me in the technical skills required, and the other members of the Wu lab, without which this thesis would not have been possible. I am also thankful for the support of my committee members, Dr. Daniel Kamei and Dr. Hsian-Rong Tseng. I would like to acknowledge the aid of Jing Wang and Dr. Wenxi Xia in Dynamic Light Scattering.

I am deeply indebted to my friends and family, who have supported me in my endeavors and whose belief in my abilities has been a source of strength and perseverance.

INTRODUCTION

By the end of 2022, kidney cancer is predicted to be the 5th most common type of cancer in the United States, after bladder, breast, colon, and rectal, and endometrial cancer [1, 2]. Current 2022 projections estimate approximately 79,000 new cases and 13,920 deaths related to kidney cancer this year. Renal Cell carcinoma or renal adenocarcinoma (RCC) accounts for 90% of kidney cancer cases. It includes a diversity of malignancies; the most common histology is Clear Cell Renal Cell Carcinoma(ccRCC), accounting for roughly 75% of RCC cases [3]. RCC prevalence has doubled over the last 50 years in the developed world, with the highest disease burden seen in North America and Western Europe [4]. As different parts of the world develop a more western lifestyle, this trend is expected to continue. Two-thirds of RCC cases are seen in men with an average age of 64 years unless there is a genetic predisposition for RCC, such as von Hippel-Lindau disease, which reduces the age of diagnosis by about 20 years. In the United States, African Americans, Hispanic Americans, and Native Americans have a greater risk of developing RCC. Risk factors for RCC include genetic predisposition based on gender, age, and race and modifiable risk factors from lifestyle such as smoking, obesity, hypertension, diet, alcohol consumption, and occupational exposures.

Survivability and initial treatment are highly dependent on the stage at diagnosis, more specifically, the tumor volume and spread beyond the kidney. If the entire tumor or the involved kidney can be removed for localized disease(stage 1) RCC, the outcome is excellent with a 5-year survival rate of 93% [4, 5]. In some cases, it is necessary to resect the entire kidney. Additional treatment options include immunotherapy and targeted therapy, including radiation, thermal ablation, and cryosurgery [5]. Regional disease(stage 2/3), which typically has lymph node

involvement, has a 5-year survival rate of 72.5%, and finally, at metastatic(stage 4) of the disease, the five-year survival rate decreases to approximately 12% [6]. About one-third of RCC patients have metastatic disease at the initial diagnosis, and 30% of patients with localized tumors have distant metastasis after surgery. Together this points to the need to develop therapies for the metastatic stage of RCC and further inquiry into the molecular mechanism of metastasis.

Loss of the von Hippel-Lindau(VHL), a tumor suppressor gene, is observed in 70% of metastatic ccRCC cases. VHL loss or mutation is a common characteristic of many human diseases, including von Hippel-Lindau hereditary cancer syndrome, development of sporadic hemangioblastomas, and ccRCC [7]. The VHL protein, pVHL, plays a role in the mammalian oxygen-sensing pathway and codes for an oxygen-dependent E3 ubiquitin ligase that binds hydroxylated HIFs and targets them for ubiquitin-mediated degradation. This reduces the HIF levels present and consequently decreases the expression of genes associated with the hypoxic response. In the absence of pVHL, HIF1A and HIF2A are stabilized and induce the expression of target hypoxic genes that regulate angiogenesis, cell growth, and cell survival, which are factors that encourage tumor growth. Tumor vascularizing factors include platelet-derived growth factor-beta(PDGFB), vascular endothelial growth factor(VEGF), and transforming growth factor-alpha [8]. The loss of pVHL in ccRCC tumor cells restricts them to a pseudo-hypoxic state with high expression of vascularizing factors. Consequently, ccRCC tumors are highly vascularized, with high metastatic potential, frequently disseminating to the lungs.

A common consequence of the loss of the VHL gene is the epithelial-mesenchymal transition(EMT) [9]. EMT is often considered a process by which metastasis occurs or that occurs concurrently. Features of EMT include loss of cell-cell contact as cells become more migratory and invasive and the loss of epithelial markers, such as E-cadherin, and the gain of mesenchymal

markers, such as N-cadherin. Morphological changes include loss of cobblestone appearance and elongation of cell shape.

Loss of the VHL gene is not uniform in clinical cases of metastatic ccRCC, and heterogeneous cell populations with both the presence and absence of VHL are observed [10]. In the absence of VHL, cell proliferation is slowed, and EMT phenotypes and molecular changes are induced. The mixing of VHL(+) and VHL(-) cells causes increased aggression and growth of VHL(+) cells. Additionally, in in vivo models with a heterogenous tumor environment of nonfunctional VHL and wild-type VHL cells, metastasis to the lungs is rampant. This suggests that there is some intercellular communication between VHL(+) and VHL(-) cells and that the VHL(-) cells must be the metastatic drivers.

Intercellular communication in the tumor-microenvironment can occur in many ways, including paracrine, endocrine, and direct cell-to-cell contact. Exosomes, a type of extracellular vesicles with a diameter range of 50 to 150 nanometers in size and are secreted by specific cell types into the extracellular space, can act locally or travel to distant sites via circulation, showing potential for both paracrine and endocrine signaling, respectively [11, 12, 13]. In hypoxic environments like tumors, cells produce increased exosomes compared to cells in a normoxic environment [14]. Exosomes have distinct cargos containing cell- and environment-specific bioactive materials that allow exosomes to act as information carriers between cells [11]. The content of exosomes is known to affect gene expression and cellular signaling pathways in recipient cells. Hypoxia-derived exosomes regulate the expression of genes associated with angiogenesis, EMT, and metastasis to promote cell survival and the adaption of cells to the hypoxia environment.

Due to the absence of a functioning VHL gene to down-regulate the hypoxic response, VHL knockout cells are in a pseudo-hypoxic state and produce more exosomes than non-pseudo-hypoxic cells, such as VHL wildtype cells [15]. Due to the increased metastasis in ccRCC tumors with mixed VHL wildtype and VHL knockout cells, exosomes may be a driver of metastasis between VHL wildtype and VHL knockout cells.

MATERIALS AND METHODS

Cell Culture

The variants of the Renca Murine cell line were cultured in RPMI 1640 1x medium (Corning, Lot #: 2852101Xontaining 10% [v/v] heat-inactivated Fetal Bovine Serum (FBS, Lot #: P101713) and 1% [v/v] PenStrep(Gibco, Lot #: 2068816). RFL_V-_54(VHL(-)) and RVN_CREX (VHL(-)-Cre) are CRISPR-modified cell lines with the knockout of the VHL gene. RFL_53 (VHL(+)) and Renca LoxP RFP (VHL(+)-LoxP) are cell lines containing the wild-type VHL gene.

Exosome Isolation and Imaging

VHL(+), VHL(-), VHL(+)-LoxP, and VHL(-)-Cre cells in T175 flasks were allowed to reach 60% confluence. At this time, the supernatant was discarded, then refreshed with 1640 1x medium with exosome depleted FBS after three sequential PBS washes and incubated over 42 hours. Exosome-depleted FBS was collected after bovine exosomes were removed via ultracentrifugation at 100,000 x g for 16 hours and filtered out of FBS. After the incubation period, the supernatant was subjected to sequential centrifugation at 300 x g for 10 min and 2000 x g for 10 min to remove cells and debris. The supernatant was then ultracentrifuged at 4^{o}C at 10,000 xg in an SWI-32-Ti swing bucket rotor (Beckman Coulter L-100XP, USA) for 30 min to remove proteins. Subsequently, the supernatant was ultracentrifuged at 4^{o}C at 100,000 x g for 1 hr 10 min to pellet exosomes. The pelleted exosomes were then resuspended in cold PBS and ultracentrifuged at 100,000 x g for 1 hr 10 min at 4°C to remove the remaining impurities. The exosome pellets were then collected by resuspension in PBS and stored at -80°C. Dynamic Light Scattering was used to determine the size and purity of collected exosomes (performed by Jing Wang and Wenxi Xia).

Cells were counted using a hemacytometer, and concentration was determined using the Bicinchoninic acid(BCA) Rapid Gold Protein Assay kit to determine the relative amount of exosomes per 10^6 cells.

Western Blotting

Samples containing cells or exosomes were lysed with RIPA buffer. Protein concentration was determined with the BCA protein kit. SDS/PAGE gels were prepared using 30% Acrylamide/Bis Solution with a 37:5:1 crosslinker ratio, and 25 ugs of cell lysates and exosomes were added to each well and ran against Tri-color Protein Marker I (10 -180 kDa, Cat. PM01) for size determination. After band separation, the gels were transferred to nitrocellulose membranes. Membranes were then subjected to a TBST blocking buffer containing 5% Bovine Serum Albumin and then incubated in primary antibodies(CD81, CD53, B-actin) at 4°C overnight. Following incubation, membranes were washed with TBST three times before the secondary antibody(mouse) was incubated for 1 hour at room temperature. Bands were visualized by enhanced chemiluminescence with a Bio-Rad ChemiDoc XRS+ imaging system.

Internalization of PKH67-labeled VHL knockout exosomes

Visualization of exosome internalization was completed using freshly isolated exosomes. PKH67 staining agent was added to 50 ug exosomes and control containing Diluent C; then, the volume was supplemented with PBS. Stained exosomes were then isolated via ultracentrifugation at 4°C 100,000 xg for 1 hr 10 min. Exosome pellets were resuspended in 1640 1x medium containing exo-free FBS. Concentrations of 0.25, 0.50, 1.25, and 2.50 ug exosomes were then added to each well of a 48-well plate with fresh 1640 1x exosome-free medium, and cells were incubated at 37°C

and 5% CO_2 for 18 hours. Images were taken at 20x magnification using the NIS-Elements AR imaging program on a fluorescent microscope.

Cre-LoxP color conversion assay

1.0 x 10^5 VHL(+)-LoxP cells were seeded onto 12-well plates. After cell adhesion overnight, the medium was discarded and replaced with 1640 1x medium containing exosome-depleted FBS containing VHL(-)-Cre exosomes in experimental groups and 1640 1x medium with exosome-depleted FBS in control groups. Images were taken at 20x magnification using the NIS-Elements AR imaging program on a fluorescent microscope.

Transwell Migration Assays

6.5 mm diameter, 8.0 um pore size, and 24-well membrane inserts (Corning, Lot #21809003) were used for Transwell migration assays. 3.0 x 10^4 cells were seeded into the upper chambers in 1640 1x medium lacking FBS. Lower chambers contained 1640 1x medium with exosome-depleted FBS and exosomes. After 36 hours of incubation, the transwell inserts were fixed with methanol and stained with 1% crystal violet. Nonmigratory cells were removed using cotton swabs. Cell counts were done in random fields under a light microscope at 10x magnification.

Wound Healing Assays

12-well plates were seeded with 2.5 x 10^5 cells and allowed to come to 90% confluence. A p-10 pipette tip was used to scratch a straight line of cells out of the center of the plate. The medium was then replaced with 1640 1x medium lacking FBS with VHL wildtype or VHL knockout exosomes added in. Pictures were taken over 42 hours at 10x magnification. Data analysis was

completed using photoshop to measure the free area between the cell borders at hours 0, 24, and 42 to determine percent migration in each sample by pixel count using Adobe Photoshop. Fluorescence microscopy was completed via time-lapse to measure color conversion and migratory effects arising from exosome internalization over a 45-hour period via time-lapse imaging at 20x magnification.

Cell proliferation assay

1.0 x 10^5 cells were seeded into each well of a flat bottom 96 well plate and incubated for 40 hours at 37°C and 5% CO2. Exosomes were added in a concentration array of 0, 0.75, 2.0, and 5.0 ug and returned to the incubator. After 42 hours, the medium was discarded and replaced with 1640 1x (no FBS) medium with 1 MTS: 10 1640 1x medium and incubated for 2 hours. Absorbance was measured at a wavelength of 490 nm using a CLARIOstar 96-well plate reader.

Duck Chorioallantoic Membrane model

Fertilized duck eggs were obtained from AA Laboratory Eggs, Incorporated. Windows of eggs were opened on developmental day 7 and sealed with Tegaderm. On developmental day 13(tumor day 0), 5.0 x 10^6 cells from VHL(-) and VHL(+) cell lines suspended in 20 ul 1640 1x medium with 10% FBS and 1% PenStrep were implanted onto a vascular-rich area of the chorioallantoic membrane of the duck embryo. This was done by using a coarse glass rod to disrupt the ectoderm and make the surface rough for implantation(performed by Junhui Hu). Four experimental groups were established: VHL(+) cells only, VHL(+) with VHL(-)-derived exosome treatment, VHL(-) cells only, and VHL(-) cells with VHL(+)-derived exosome treatment. Exosomes were added on developmental days 15, 17, 19, and 21(tumor days 2, 4, 6, 8, and 10) in 80 ug doses directly to the

tumor surface. On developmental day 26(tumor day 13), eggs were euthanized after being anesthetized by isoflurane inhalation. Tumors and kidneys were collected for analysis via qPCR. Tumor weights and sizes were measured on the day of euthanasia.

DNA isolation and quantitative PCR

Genomic DNA was extracted from tumor and kidney samples collected from the dCAM groups by phenol-chloroform liquid-liquid phase extraction, precipitated with 100% ethanol and 70% ethanol to remove salts. After 5 min centrifugation at 12,000 xg to pellet the genomic DNA, samples were resuspended in ddH_2O. To complete quantitative PCR (qPCR); Master mix, ddH_2O, and ß-actin probes for chicken and mouse(Gg03815934_s1 ACTB, Mm02619580_g1 Actb) were used to make the reaction mixtures. Genomic DNA was then added to the reaction mixture and amplified on the Quantstudio5 instrument. Relative fold expression of mouse ß-actin to avian ß-actin was determined using the $2^{-\Delta\Delta Ct}$ method.

Statistical Analysis

Statistical Analysis was performed using GraphPad Prism 9.3.1. Quantitative data is displayed using means and standard deviations. Significant statistical differences are shown using asterisks (* $p < 0.05$, ** $p < 0.01$, *** $p < 0.001$, **** $p < 0.0001$).

RESULTS AND DISCUSSION

The Wu lab discovered that VHL expression is often heterogeneous in ccRCC tumors. To understand the impact of this heterogeneity, the lab generated a VHL(-) line from the VHL (+) wildtype Renca cell line using a CRISPR approach [9]. The Renca cell line is derived from a spontaneously arising renal tumor in a Balb/C mouse. Intriguingly, fulminant lung metastases only occurred when both VHL(-) and VHL(+) Renca cells are co-implanted into the mouse kidney. Implanting either cells alone do not result in metastasis. This result strongly suggested that cross communications between the two cell populations are inducing metastasis. This thesis project aims to investigate whether exosomes could be mediating the metastatic crosstalk communication.

The physical and biochemical character of the exosomes were first examined in detail in VHL(-) and VHL (+) Renca cells and the VHL(-)-Cre cells and the VHL(+)-LoxP cells. The two pairs of cell lines are syngeneic except for the insertion of a Cre-LoxP reporter system to track the exosomal transfer between the two cells. Following characterization of exosomes, the Cre-LoxP system and staining techniques were employed to determine a relative period of exosome uptake and functionalization in recipient cells. In vitro methodologies to assess cell migration and proliferation were then utilized to determine the effect of VHL knockout-derived exosomes on migration and proliferation of VHL wildtype cells. Finally, distant metastasis to the liver was evaluated using the duck Chorioallantoic membrane model (dCAM).

1. Physical and Biochemical Characterization

After exosome collection, size analysis using Dynamic Light Scattering(DLS) was completed to

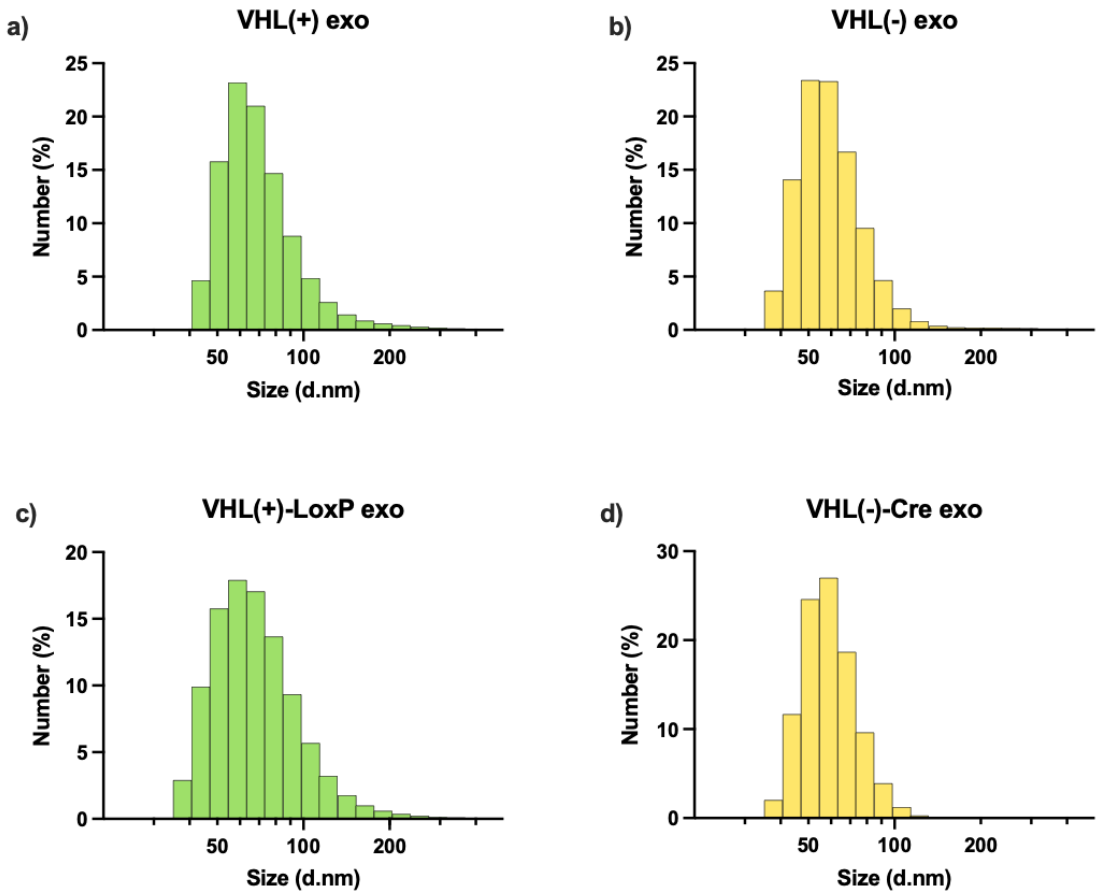

Figure 1: Dynamic Light Scattering of tumor cell exosomes. Exosomes isolated from VHL wildtype **a)** VHL(+) and **c**) VHL(+)-LoxP and VHL knockout **b)** VHL(-) and **d)** VHL(+)-Cre cell lines.

determine the size distribution profile of suspended exosomes **(Fig. 1)**. DLS results showed a Gaussian exosome size distribution from 50 to 150 nanometers from all cell types, falling within the expected size range of exosomes. DLS number measurements were used for analysis as intensity measurements tend to show bimodal trends likely due to exosome aggregation within the sample measured and cloud results of individual exosome size. Of the VHL knockout exosomes, the highest proportion of VHL(-) and VHL(-)-Cre exosomes were 50.7 nm and 58.8 nm,

respectively, and within the VHL wildtype exosomes, the highest proportion of VHL(+) and VHL(+)-LoxP-exosomes were 58.8 nm. In all exosome samples, the exosome purity was high, as indicated by the peak size of DLS measurements and the low standard deviation from the mean.

To confirm that exosomes and no other extracellular proteins were isolated from these

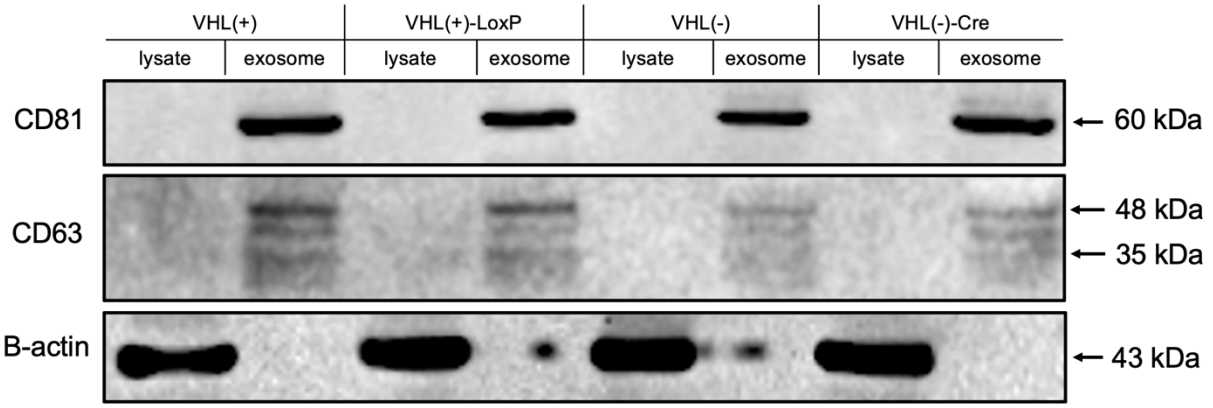

Figure 2: Western Blot for Exosome Markers, CD81 and CD63. Cell lysates compared to corresponding isolated exosomes. ß-actin as loading control.

exosome isolation procedures, western blotting was employed using primary antibodies for classical exosome markers, CD63 and CD81 **(Fig. 2)**. CD63 and CD81 are common membrane-spanning tetraspanins that are enriched in exosome membranes. Strong bands for CD63 and CD81 were seen in exosome samples compared to cell lysates from corresponding cell lines, confirming that the exosome isolation protocol is tuned for efficient isolation of exosomes. Multiple bands for CD63 are seen due to the multiple glycosylated isoforms of CD63 that are generated via post-translational modifications. As a control, ß-actin primary antibodies were tested for cell lysates and their corresponding exosomes. ß-actin is a cytoskeletal component in all eukaryotic cell types but is typically absent in exosomes as they lack a cytoskeleton. Strong bands were seen solely in cell lysate samples and not in exosome samples, suggesting effective

exosome isolation from cellular components.

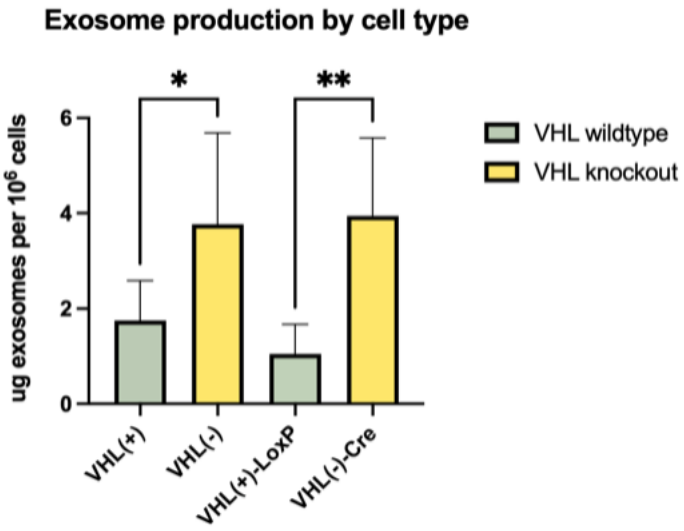

Figure 3: Exosome production of tumor cells. Increased exosome production in cells with knockout of VHL gene compared to cells with wildtype VHL gene.

At collection time, the concentration of exosomes per total cell number from cell types with VHL wild type and VHL knockout significantly differed **(Fig. 3)**. VHL wildtype cells, VHL(+) and VHL(+)-LoxP, on average, produced 1.75 and 1.05 ug exosomes per 10^6 cells, while VHL knockout cells, VHL(-) and VHL(-)-Cre, on average typically produced 3.77 and 3.94 ug exosomes per 10^6 cells. Since VHL knockout cells are in a pseudo-hypoxic state due to the up-regulation of the HIF1a and HIF2a genes that activate hypoxia-response gene sets, these concentrations support previous studies claiming that cells in a more hypoxic environment generate more extracellular vesicles and that VHL knockout cells also have increased exosome production compared to VHL wildtype cells [15].

2. *Exosome uptake*

To ascertain the location of action of exosomes collected, PKH67-staining of exosomes, DAPI-staining, and F-actin-staining was completed **(Fig. 4ab)**. After an 18-hour incubation, exosomes can be seen inside the cell as the green fluorescence is localized within the cytoplasm instead of at the cell membrane where F-actin staining of fibrous actin in the cytoskeleton is prevalent.

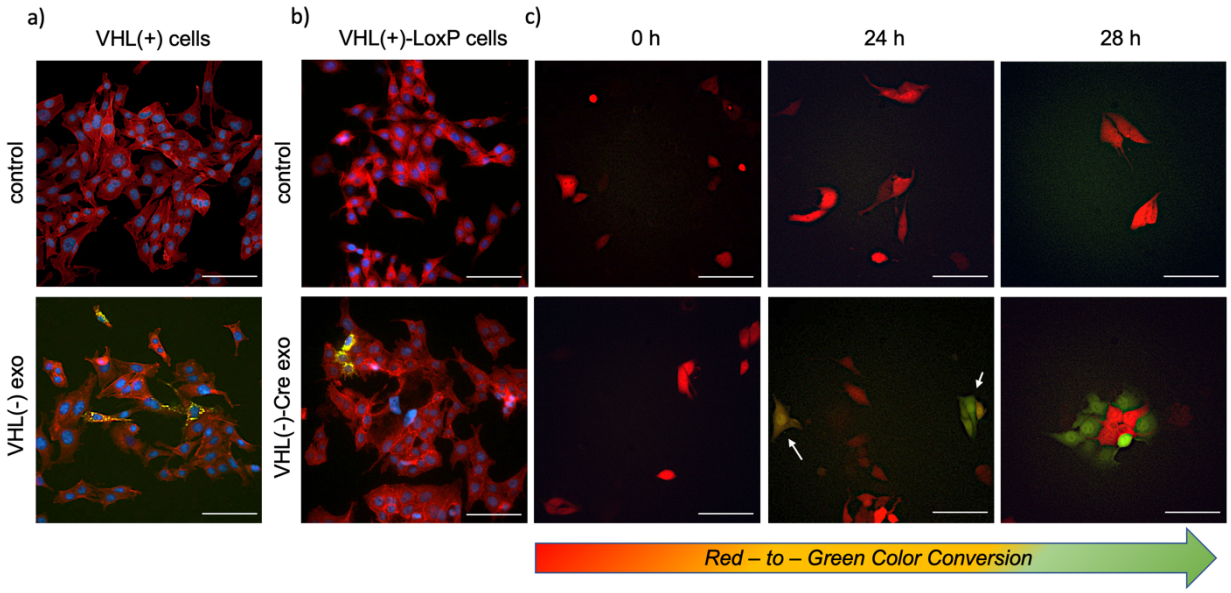

Figure 4: Exosome uptake in tumor cells. a) & b) VHL knockout exosome internalization into VHL wildtype cells, a) VHL(-) exosomes into VHL(+) cells and b) VHL(-)-Cre exosomes into VHL(+)-LoxP cells, via PKH67 staining of exosomes. Fixed after 18-hour incubation and cross-stained with F-actin and DAPI. c) Color conversion of VHL(+)-LoxP cells from red to green fluorescence upon incubation of VHL(-)-Cre exosomes over a 28-hour time course. Arrows indicate cells in process of color conversion. Scale bars = 100 µm.

This suggests that 18 hours is sufficient for internalization of exosomes into the cell. To assess if internalized exosomes have a functional effect inside the cell, the CRE-LoxP system was employed **(Fig. 4c)**. The Cre-LoxP system has Cre recombinase inserted into the VHL(-) cells, resulting in VHL(-)-Cre cells, while the VHL(+)-LoxP cells contained genes with red fluorescent protein followed by a stop signal and then green fluorescent protein gene (RFP-STOP-GFP). In

this system, the VHL(-)-Cre tumor cell releases vesicles containing Cre recombinase. The uptake of these vesicles by the VHL(+)-LoxP cells will convert the color of the cells from red to green fluorescence via the function of Cre recombinase [15]. The color of VHL(+)-LoxP cells undergoes color conversion when introduced to VHL(-)-Cre-VHL(-) exosomes, suggesting internalization of the Cre-recombinase vesicles and removal of RFP via recombination. At time 0, the LoxP cells maintain expression of RFP; after 24 hours, some cells have completed the color change and are expressing GFP, while other cells still likely express both RFP and GFP and appear yellow-orange suggesting a color change in progress. This provides a 24-hour window for exosomes to internalize and become functional in recipient cells. At hour 28, the number of cells expressing GFP increases suggesting that more VHL(+)-LoxP cells have completed the Cre-induced color conversion. The period of exosome uptake and consequent functionality requires further validation to rectify the difference between 18-hour and 24-hour time points in incubations. This difference is likely due to experimental variations in exosome concentration and cell seeding density as well as the period of required for the Cre recombinase to alter fluorescence after the vesicle enters the cell.

3. In vitro Functionality

Migration

Increased migratory ability is a common characteristic of metastatic cancer. To assess exosome ability to increase two-dimensional migration, VHL(+) cells and VHL(-) cells were treated with

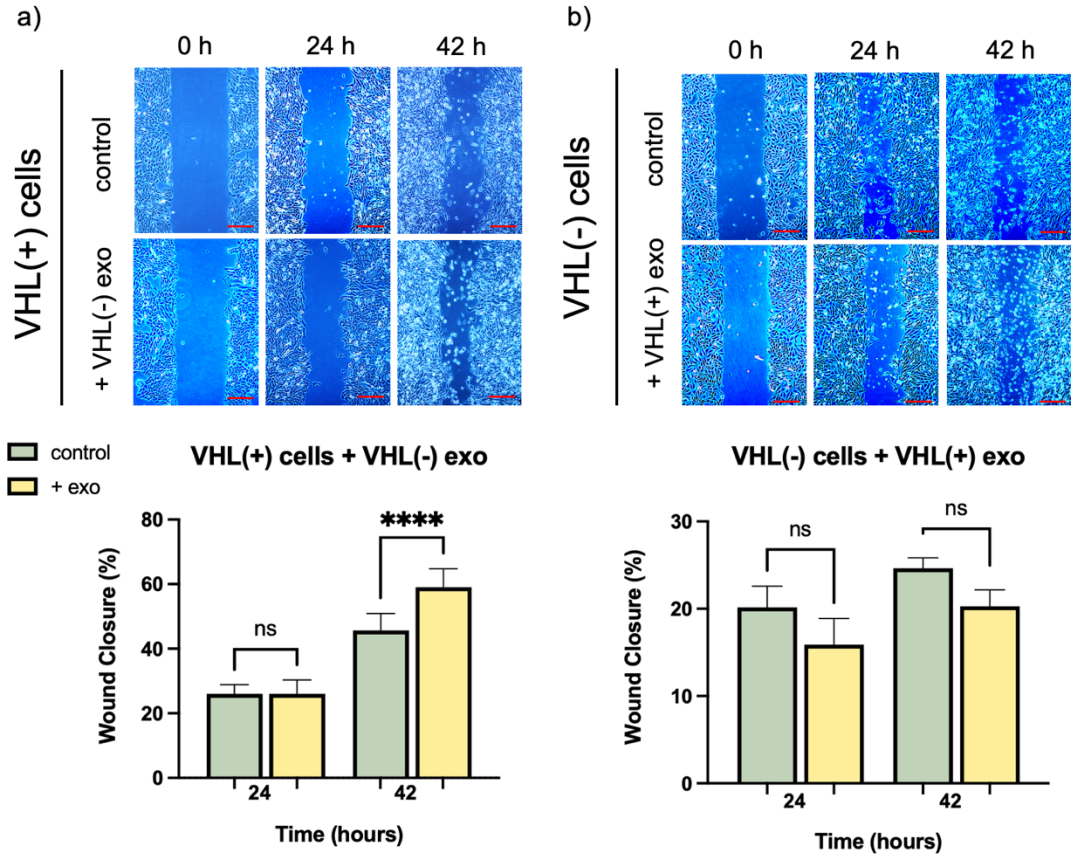

Figure 5: Tumor-derived exosome effects on two-dimensional migration. Wound Healing assay of VHL(+) cells in response to VHL(-) exosomes and VHL(-) cells in response to VHL(+) exosomes over the course of 42-hour incubation. Imaged at 10x magnification on a light microscope. Scale bars = 500µm.

VHL(-) and VHL(+) exosomes, respectively **(Fig. 5)**. Over the course of 42 hours, VHL(+) cells with VHL(-) exosome treatment had increased two-dimensional migration compared to the control group of VHL(-) cells without exosomes added **(Fig. 5a)**. At 24 hours, there was no significant

difference between the control and experimental groups, likely due to the approximately 24-hour exosome internalization-functionalization period. The exosomes only had a discernible effect on VHL(+) cells over the last 18 hours of the incubation. Additionally, VHL(-) cells treated with

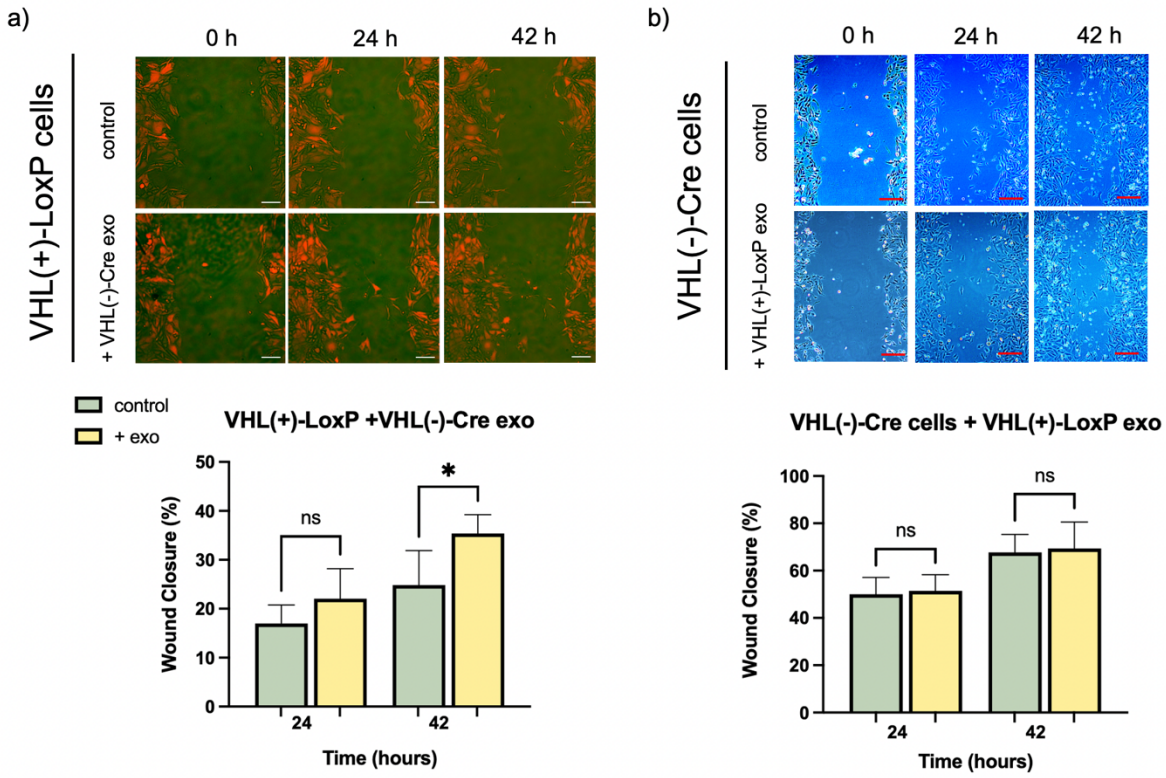

Figure 6: Tumor-derived exosome effects on two-dimensional migration using Cre-LoxP cell lines. Wound Healing assay of a) VHL(+)-LoxP cells in response to VHL(-)-Cre exosomes and b) VHL(-)-Cre cells in response to VHL(+)-LoxP exosomes over the course of 42-hour incubation. Imaged at a) 20x and b) 10x magnification on a) fluorescent and b) light microscope. Scale bars = a) 100 µm and b) 500 µm.

VHL(+) exosomes had no difference between the control and experimental groups **(Fig. 5b)**.

VHL(+)-LoxP cells were incubated with VHL(-)-Cre exosomes to observe Cre-induced color conversion during wound healing assay using time-lapse fluorescent microscopy **(Fig. 6a)**. Although color conversion did not occur this is likely due to a large percentage of VHL(-)-LoxP cells not expressing the RFP-STOP-GFP code. Further selection with puromycin, a selective marker for VHL(+)-LoxP cells will optimize the levels of RFP-expressing VHL(+)-LoxP cells. Despite exosome internalization lacking color conversion, there was still a statistically significant

increase in two-dimensional migratory capabilities of VHL(+)-LoxP cells. Compared to control VHL(+)-LoxP cells without exosome treatment, wound closure was increased in VHL(-)-Cre exosome groups. VHL(-)-Cre cells with VHL(+)-LoxP exosome supplemented media had no significant difference from control groups lacking exosomes **(Fig.6b).** These results are consistent

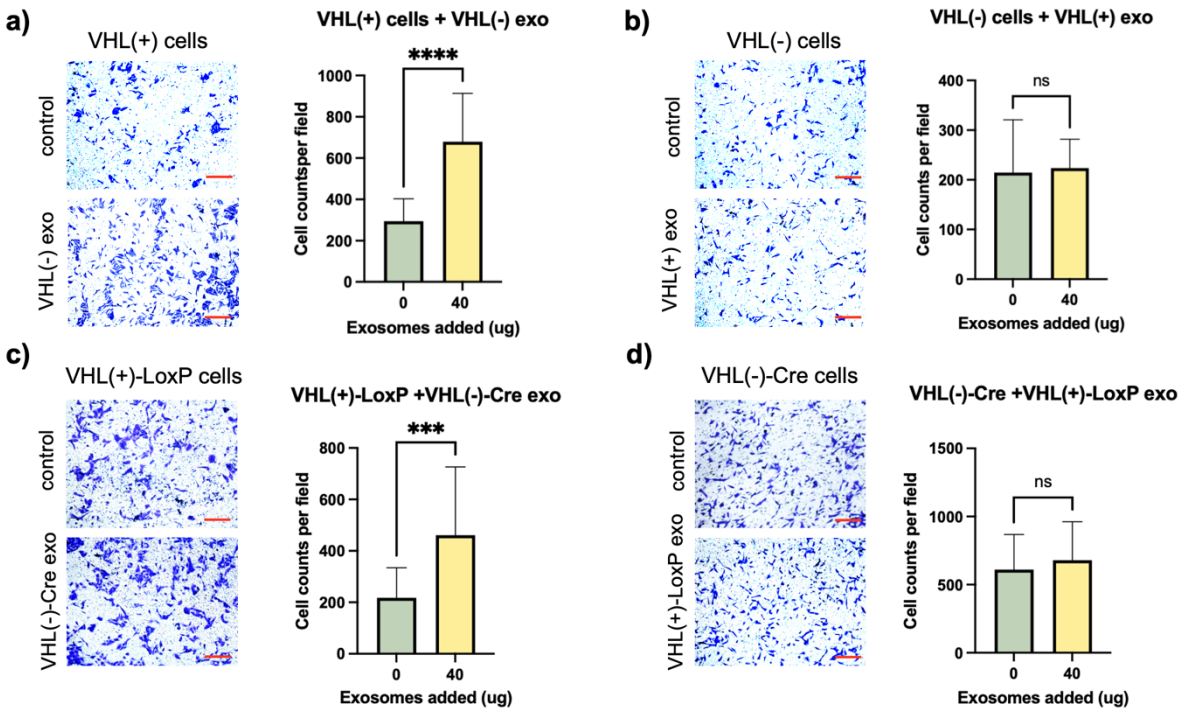

Figure 7: Tumor-derived exosome effects on chemotactic migration. Transwell migration assays of VHL(+) cells in response to VHL(-) exosomes and VHL(-) cells in response to VHL(+) exosomes after 36-hour incubation. Imaged at 10x magnification on a light microscope. Scale bars = 500 µm.

with those seen in VHL(-) and VHL(+) wound healing experiments and suggest that while wildtype VHL exosomes have no effect on migration, VHL knockout exosomes increase the two-dimensional migration of VHL wildtype cells.

The three-dimensional migration capability of VHL(+) and VHL(-) ccRCC cells was tested by comparison of chemotaxis to exo-depleted FBS in the absence and the presence of VHL knockout and VHL wildtype exosomes **(Fig. 7)**. In the presence of VHL(-)-derived exosomes, VHL(+) cells have increased migratory abilities. Additionally, it was seen that there was no

significant effect of VHL(+)-derived exosomes on VHL(-) cells. These effects were consistent in VHL(+)-LoxP having increased directional migration in response to exosomes derived from VHL(-)-Cre cells.

Proliferation

Cell proliferation of both VHL(+) and VHL(+)-LoxP cells in response to VHL(-) and VHL(-)-Cre exosomes remained unchanged after 45-hour incubation via MTS Tetrazolium Assay **(Fig. 8)**.

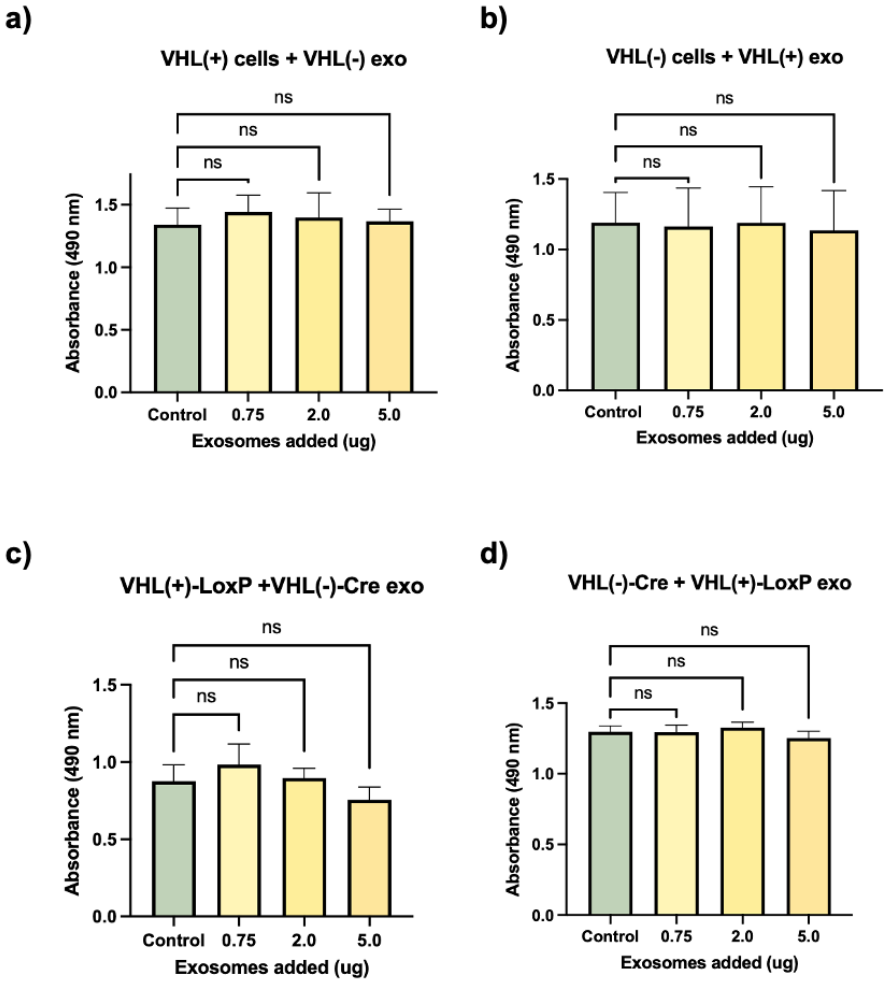

Figure 8: Tumor-derived exosome effects on cell proliferation. Cell Proliferation of VHL wildtype and VHL knockout cells in response to VHL knockout and VHL wildtype exosomes by change in absorbance at 490 nm.

This suggests that both VHL wildtype and VHL knockout exosomes do not play a role in regulating cell division.

4. In vivo Functionality

VHL(+) and VHL(-) cell lines were employed to assess in vivo tumor growth and metastasis in a duck Chorioallantoic membrane model (dCAM). CAM models provide a less expensive, and less time-consuming model than immunocompromised mice [16]. The dCAM model has a tumor growth window of two weeks after implantation, providing a window of metastasis within the

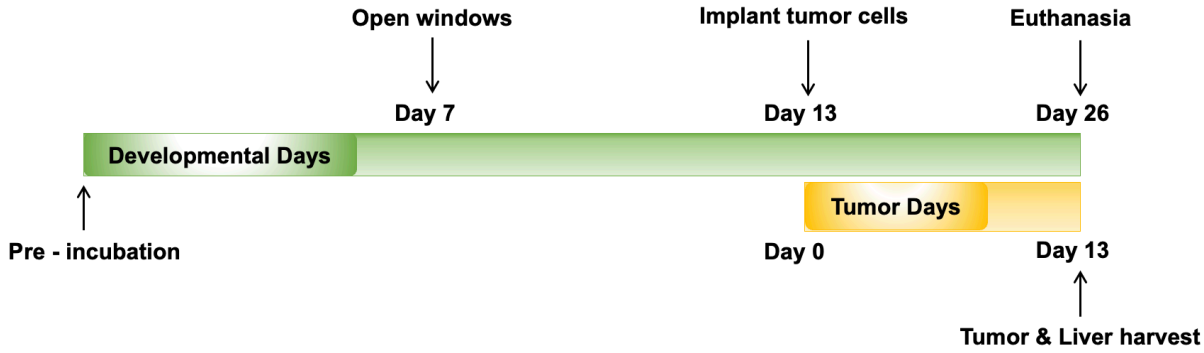

Schematic 1: Duck chorioallantoic membrane model experimental timeline

embryo prior to euthanasia **(Sch. 2)**. Four groups were used, VHL(+) cells only, VHL(+) cells with VHL(-) exosomes, VHL(-) cells only, and VHL(-) cells with VHL(+) exosomes. Treatment of tumors with exosomes was given five times throughout the remaining developmental window to account for high cell numbers in the tumor, possible minimal effective internalization, and the possible loss of exosome suspension to non-tumor areas. Additionally, treatment was given every 48 hours to provide a window for internalization and functionality before the subsequent treatment.

On the day of euthanasia, vascularized tumors in every group had significant variations in size, with some lacking tumors, possibly due to errors in implantation strategy or loss of cell viability during implantation. Due to proliferation experiments, tumor size was not expected to depend on exosome treatment as no significant proliferative effect was observed in vitro. Livers are a highly vascularized part of the duck embryo and have high potential as a metastatic site. This

differs from clinical ccRCC in humans, where lung metastasis is the most common metastatic site. Prior to hatching, the lungs have not inflated and are less vascularized than the liver and consequently are less likely to be a metastatic site.

Duck embryo livers were collected and quantified via qPCR to observe in vivo metastasis of tumor VHL(+) cells. qPCR of livers using murine and avian probes allowed the determination of a ratio of relative murine to avian DNA expression in each group. Compared to the control VHL(+) cell-only group, the VHL(+) cells with VHL(-) exosomes had a higher mouse to avian ß-actin ratio with an average fold change in murine DNA expression of 8.445, while there were minimal differences in mouse to avian expression in livers from VHL(-) cells only to VHL(-) cells with VHL(+) exosomes, with several groups having non-detectable amounts of murine DNA observed and on average there was fold change of 0.0582 between control and experimental groups. This result suggests that VHL(-) exosomes are increasing metastasis of VHL(+) cells to the liver. Furthermore, these results suggest that VHL(+) exosomes do not play a role in increasing VHL(-) metastasis. Due to the high variation in tumor sizes and limited sample sizes of this dCAM experiment, further experimentation is needed to optimize experimental conditions and confirm the results' significance.

CONCLUSION

Thus far, when VHL wildtype cells and VHL knockout derived exosomes are present, there have been increased metastatic properties. A possible mechanism of RCC metastasis is uptake of VHL knockout exosomes either at the tumor site or traveling via vasculature to a metastatic site

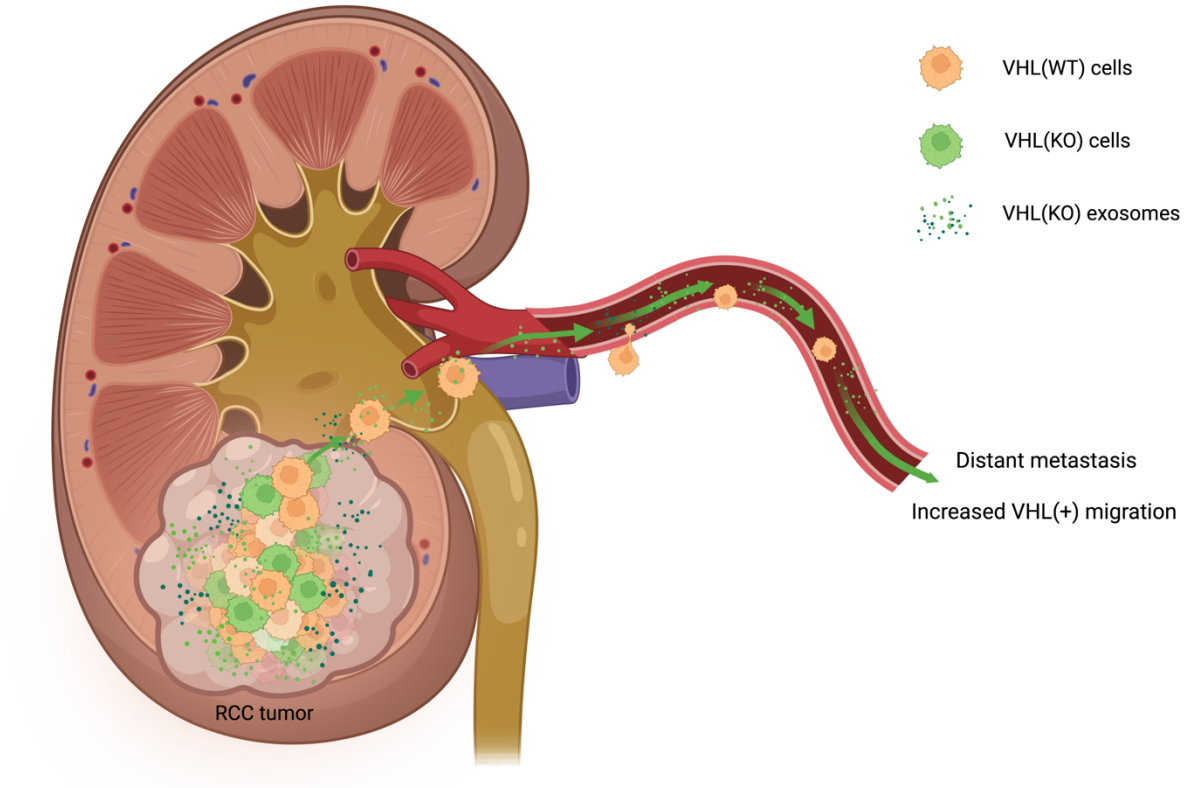

Schematic 2: Proposed mechanism of RCC metastasis. Communication between VHL(WT) cells and VHL(KO) exosomes. Adapted from "Tumor Cell Metastasis", by BioRender.com(2020). Retrieved from https://app.biorender.com/biorender-templates

and subsequently increasing the migration abilities of VHL wildtype cells **(Sch. 2)**. With the confirmation of the metastatic effects of VHL knockout-derived exosomes on VHL wildtype cells, we are one step further to understanding the molecular mechanism of metastasis in ccRCC. This

provides downstream bench-side to bed-side possibilities in diagnosing and treating metastatic kidney cancer via biomarkers and bioactive components in the exosomes.

Due to the lipid bilayer that surrounds exosomes, they are stable in many body fluids, including blood, plasma, serum, urine, and saliva, providing the possibility for a minimally invasive method of diagnosing and monitoring patients with metastatic kidney cancer that could be incorporated into a regular doctors visit which will decrease late-stage diagnosis of metastatic malignancies [17]. Currently, plasma has had the most significant potential for detecting solid tumors. As of 2019, several studies are investigating the correlation between exosome plasma concentration and tumor burden, pre-and post-treatment. For example, CD63 and caveolin-1 (CAV1) expressing exosomes in stage IV oral squamous cell carcinoma were higher in patients with active tumor progression and decreased in patients with long-term survival. Furthermore, an exosome-based diagnosis could provide a way of discerning between benign or malignant cancers or confirming diagnosis based on the presence of biomarkers associated with tumor progression. Understanding tumor heterogeneity and the most deregulated proteins associated with metastatic ccRCC are necessary to develop an exosome-based diagnostic tool [17]. Current limitations to success in this field are the labor-heavy, time-consuming processes involved in exosome harvest and isolation and associated costs. Additionally, exosome quantification via enzyme-linked immunosorbent assay(ELISA), flow cytometry, and nanoparticle tracking analysis(NTA) have myriad complications, including high background noise or contaminants, inconsistent results, time-consuming processes, and require expensive equipment that is not available in resource-limited clinical settings [18].

Microfluidic chips and nano-sensing devices are being developed for exosome-based diagnostic tools to overcome these limitations. An example of an electrochemical device, called

IMEX, uses magnetic beads functionalized with CD9, CD63, and CD81 to capture exosomes and pull bead-captured exosomes to the electrodes for electromagnetic sensing. This system could be optimized for different cancers using cancer-specific exosome marker antibodies. Microfluidic methods could also circumvent exosome-based challenges and provide cost-effective rapid results with minimal sample size required. However, microfluidic chips require skilled individuals for proper use and have limited potential for automation. Additionally, nanosensors have the potential for real-time monitoring and identification of multiple cancer-specific markers but are limited due to reproducibility issues in their fabrication.

Currently, many technologies are in progress to increase the collection of pure samples of cancer-specific exosomes for downstream analysis of mRNA, one of which is the use of "Click Beads", which uses lipid-labeling and click chemistry-based techniques for extracellular vesicle capture [19]. With this convenient and efficient method, cancer-specific exosome isolation will be enhanced, providing increased purity to determine cancer-specific exosome contents with techniques like RT-qPCR and ability to perform liquid biopsy of cancer-specific exosomes found in the body. Determination of exosome contents will further circumvent the limitations associated with exosome isolation, characterization, and quantification in the clinic setting and aid in to developing diagnostic strategies for exosome contents, such as microRNAs (miRNAs). miRNAs are short non-coding RNAs that target and repress complementary mRNAs. miRNAs have known functions in differentiation, proliferation, and cell cycle regulation. Electrochemical sensing of miRNAs has been done using locked-nucleic-acids (LNA) and bipedal DNA walkers to increase the binding of miRNA sequences [17]. The use of biosensors in clinical settings has the potential for sensitive and precise real-time detection while also being portable and cost-effective. Limitations include initial fabrication and production for specific and reproducible results.

In addition to diagnostic potential, cancer-specific exosomes and their bioactive contents provide a potential therapeutic target for metastatic disease in response to an initial diagnosis or long-term preventative measures in patients with a high risk of developing RCC [20]. Two possibilities currently being pursued in research are targeting the cancer-specific exosomes to impede their communication abilities or using them for the delivery of therapeutic agents such as chemotherapies for specific and targeted drug release.

Targeting of cancer-specific exosomes to reduce their metastatic potential aims to eliminate exosomes from circulation, inhibit their secretion, or prevent their internalization into recipient cells [21]. Inhibitors of exosome production target the pathways involved in the production of multi-vesicular bodies(MVB), including ESCRT-dependent and ESCRT-independent pathways [22]. These pathways are associated with RAS GTPase and nSMase proteins and the potential inhibitors, Manumycin and GW4869, are being investigated as both experimental tools and therapeutic approaches to halt disease progression. More proposed inhibitors of exosome production and secretion are those that target the Calpain family proteins, which are calcium-dependent neutral, cytosolic cysteine proteases that have roles in microvesicle shedding. Limitations of exosome inhibition include side effects arising from stopping EV release from healthy cells and therapies would need development to specifically target tumor cell-derived exosomes.

Artificially created exosomes are also being considered as drug delivery vehicles for a targeted and specific release of therapeutic drugs or bioactive elements [23]. After cancer-specific exosome biomarkers are determined they can be functionalized at the surface of engineered exosomes to act as targeting ligands for the recipient tumor cells, minimizing off-target drug effects of drugs. For example, an engineered exosome drug delivery system was generated for

treatment of breast cancer with target anti-cancer chemotherapy via doxorubicin and functionalized with an iRGD peptide as a targeting ligand [23]. Using exosomes as therapeutic nanocarriers takes advantage of the enhanced permeability and retention(EPR) effect that is theorized with nanoparticle drug delivery systems, where i.v. administered nanocarriers have the tendency to accumulate due to leaky vasculature, and defective lymphatic drainage at the tumor site while having significantly lower concentrations in the blood plasma [24]. The combination of ligand-targeted and EPR effect passive accumulation of nanocarriers at the tumor site should reduce side effects associated with off-target drug actions. Furthermore, by employing acid-dependent degradation of nanocarriers, degradation can be tuned to the acidic tumor microenvironment.

Further comprehension of the metastatic crosstalk occurring between VHL(-) exosomes and their recipient VHL(+) cells provides the potential for developing diagnostic and therapeutic strategies for the metastatic stage of RCC. Early and consistent diagnosis of metastatic disease and targeted therapeutic delivery will improve patient outcomes and provide insights into the metastatic stage of other cancers.

FUTURE DIRECTIONS

To further increase understanding of the mechanism of metastasis in RCC, another property to test is the invasion capabilities of VHL(+) cells introduced to VHL(-) exosomes. Additionally, comparison of VHL(+) cells with VHL(-) exosomes to a positive control of mixed cell populations of VHL(-) to VHL(+) cells in a 1:1 ratio to observe if VHL(-) exosomes recapitulate the effects of mixed cell populations. Furthermore, this control could be reversed by adding an exosome inhibitor to these mixed groups to see if the metastatic effects could be inhibited in VHL(-): VHL(+) co-culture by inhibiting exosome production. Branching into human cell lines will confirm that the impacts of VHL(-) exosomes are not specific to the murine Renca line and have clinical relevance. Furthermore, additional in vivo experimentation needs to be performed in CAM models and immunocompromised mice. Determination of bioactive molecules and exosome-specific biomarkers in the VHL(-)-derived exosomes will help further the understanding of the metastatic mechanism and how this mechanism can be used for diagnostics and therapeutic development.

REFERENCES

1. Feng, X., Zhang, L., Tu, W., & Cang, S. (2019). Frequency, incidence and survival outcomes of clear cell renal cell carcinoma in the United States from 1973 to 2014: A SEER-based analysis. *Medicine*, *98*(31), e16684. https://doi.org/10.1097/MD.0000000000016684

2. Siegel, R. L., Miller, K. D., Fuchs, H. E., & Jemal, A. (2022). Cancer statistics, 2022. *CA: A Cancer Journal for Clinicians*, *72*(1), 7–33. https://doi.org/10.3322/caac.21708

3. Atkins, M. B., & Tannir, N. M. (2018). Current and emerging therapies for first-line treatment of metastatic clear cell renal cell carcinoma. *Cancer Treatment Reviews*, *70*, 127–137. https://doi.org/10.1016/j.ctrv.2018.07.009

4. Padala, S. A., Barsouk, A., Thandra, K. C., Saginala, K., Mohammed, A., Vakiti, A., Rawla, P., & Barsouk, A. (2020). Epidemiology of Renal Cell Carcinoma. *World Journal of Oncology*, *11*(3), 79–87. https://doi.org/10.14740/wjon1279

5. Hsieh, J. J., Purdue, M. P., Signoretti, S., Swanton, C., Albiges, L., Schmidinger, M., Heng, D. Y., Larkin, J., & Ficarra, V. (2017). Renal cell carcinoma. *Nature Reviews. Disease Primers*, *3*, 17009. https://doi.org/10.1038/nrdp.2017.9

6. Mattila, K. E., Vainio, P., & Jaakkola, P. M. (2022). Prognostic Factors for Localized Clear Cell Renal Cell Carcinoma and Their Application in Adjuvant Therapy. *Cancers*, *14*(1), 239. https://doi.org/10.3390/cancers14010239

7. Kim, W. Y., & Kaelin, W. G. (2004). Role of VHL Gene Mutation in Human Cancer. *Journal of Clinical Oncology*, *22*(24), 4991–5004. https://doi.org/10.1200/JCO.2004.05.061

8. Padala, S. A., & Kallam, A. (2022). Clear Cell Renal Carcinoma. In *StatPearls*. StatPearls Publishing. http://www.ncbi.nlm.nih.gov/books/NBK557644/

9. Schokrpur, S., Hu, J., Moughon, D., Liu, P., Lin, L., Hermann, K., Mangul, S., Guan, W., Pellegrini, M., xu, H., & Wu, L. (2016). CRISPR-Mediated VHL Knockout Generates an Improved Model for Metastatic Renal Cell Carcinoma. *Scientific Reports*, *6*, 29032. https://doi.org/10.1038/srep29032

10. Hu, J., Tan, Ping, Ishihara, Moe, Bayley, Nicholas, Schokrpur, Shiruyeh, Reynoso, Jeremy, Jat, Parmjit, Van Snick, Jacques, Knudsen, Beatrice, Chin, Arnold, Prins, Robert, Graeber, Thomas, Xu, Hua, & Wu, Lily. (2021, September 10). *Tumor Heterogeneity in VHL Drives Metastasis in Clear Cell Renal Cell Carcinoma*. https://doi.org/10.21203/rs.3.rs-846239/v1

11. Sun, Z., Wang, L., Dong, L., & Wang, X. (2018). The emerging role of exosome signaling in maintaining cancer stem cell dynamic equilibrium. *Journal of Cellular and Molecular Medicine*, *22*(8), 3719–3728. https://doi.org/10.1111/jcmm.13676

12. Maia, J., Caja, S., Strano Moraes, M. C., Couto, N., & Costa-Silva, B. (2018). Exosome-Based Cell-Cell Communication in the Tumor Microenvironment. *Frontiers in Cell and Developmental Biology*, *6*. https://www.frontiersin.org/article/10.3389/fcell.2018.00018

13. Willms, E., Cabañas, C., Mäger, I., Wood, M. J. A., & Vader, P. (2018). Extracellular Vesicle Heterogeneity: Subpopulations, Isolation Techniques, and Diverse Functions in Cancer Progression. *Frontiers in Immunology*, *9*. https://www.frontiersin.org/article/10.3389/fimmu.2018.00738

14. Shao, C., Yang, F., Miao, S., Liu, W., Wang, C., Shu, Y., & Shen, H. (2018). Role of hypoxia-induced exosomes in tumor biology. *Molecular Cancer*, *17*, 120. https://doi.org/10.1186/s12943-018-0869-y

15. Bister N, Pistono C, Huremagic B, Jolkkonen J, Giugno R, Malm T. Hypoxia and extracellular vesicles: A review on methods, vesicular cargo and functions. J Extracell Vesicles. 2020;10:e12002. https://doi.org/10.1002/jev2.12002

16. Hu, J., Ishihara, M., Chin, A. I., & Wu, L. (2019). Establishment of xenografts of urological cancers on chicken chorioallantoic membrane (CAM) to study metastasis. *Precision clinical medicine*, *2*(3), 140–151. https://doi.org/10.1093/pcmedi/pbz018

17. Makler, A., & Asghar, W. (2020). Exosomal biomarkers for cancer diagnosis and patient monitoring. *Expert Review of Molecular Diagnostics*, *20*(4), 387–400. https://doi.org/10.1080/14737159.2020.1731308

18. Yu, D., Li, Y., Wang, M., Gu, J., Xu, W., Cai, H., Fang, X., & Zhang, X. (2022). Exosomes as a new frontier of cancer liquid biopsy. *Molecular Cancer*, *21*(1), 56. https://doi.org/10.1186/s12943-022-01509-9

19. Sun, N., Tran, B. V., Peng, Z., Wang, J., Zhang, C., Yang, P., Zhang, T. X., Widjaja, J., Zhang, R. Y., Xia, W., Keir, A., She, J., Yu, H., Shyue, J., Zhu, H., Agopian, V. G., Pei, R., Tomlinson, J. S., Toretsky, J. A., … Zhu, Y. (2022). Coupling Lipid Labeling and Click Chemistry Enables Isolation of Extracellular Vesicles for Noninvasive Detection of Oncogenic Gene Alterations. *Advanced Science*, *9*(14), 2105853. https://doi.org/10.1002/advs.202105853

20. Thind, A., & Wilson, C. (2016). Exosomal miRNAs as cancer biomarkers and therapeutic targets. *Journal of Extracellular Vesicles*, *5*(1), 31292. https://doi.org/10.3402/jev.v5.31292

21. Amoah Barnie, P., Afrifa, J., Ofori Gyamerah, E., & Amoani, B. (2022). Extracellular Vesicles as Biomarkers and Therapeutic Targets in Cancers. In *Physiology* (Vol. 0). IntechOpen. https://doi.org/10.5772/intechopen.101783

22. Catalano, M., & O'Driscoll, L. (2020). Inhibiting extracellular vesicles formation and release: A review of EV inhibitors. *Journal of Extracellular Vesicles*, *9*(1), 1703244. https://doi.org/10.1080/20013078.2019.1703244

23. Liang, Y., Duan, L., Lu, J., & Xia, J. (2021). Engineering exosomes for targeted drug delivery. *Theranostics*, *11*(7), 3183–3195. https://doi.org/10.7150/thno.52570

24. Subhan, M. A., Yalamarty, S. S. K., Filipczak, N., Parveen, F., & Torchilin, V. P. (2021). Recent Advances in Tumor Targeting via EPR Effect for Cancer Treatment. *Journal of Personalized Medicine*, *11*(6), 571. https://doi.org/10.3390/jpm11060571